Non-Back-Drivable Rotary Mechanism with Intrinsic Compliance for Robotic Thumb Abduction/Adduction

F. Montagnani, M. Controzzi, C. Cipriani

Non-Back-Drivable Rotary Mechanism with Intrinsic Compliance for Robotic Thumb Abduction/Adduction

Federico Montagnani[*]

The BioRobotics Institute, Scuola Superiore Sant'Anna, Italy.

V.le R. Piaggio, 34
56025 Pontedera (PI) – Italy
f.montagnani@sssup.it

Marco Controzzi[*c]

The BioRobotics Institute, Scuola Superiore Sant'Anna, Italy.

V.le R. Piaggio, 34
56025 Pontedera (PI) - Italy
marco.controzzi@sssup.it

Christian Cipriani

The BioRobotics Institute, Scuola Superiore Sant'Anna, Italy.

V.le R. Piaggio, 34
56025 Pontedera (PI) - Italy
ch.cipriani@sssup.it

[*] equal contribution
[C] corresponding author

Non-Back-Drivable Rotary Mechanism with Intrinsic Compliance for Robotic Thumb Abduction/Adduction

Duplicating the complexity of the human thumb with a robotic one is a difficult task for engineers, when taking into consideration the necessary miniaturization and robustness requirements. Miniaturization is required to fit all the components within the size of a human hand, however the reduction in size of the components affects the strength of the transmission. Several robotic hands with active thumbs were designed. Most of these had the abduction/adduction joint rigidly connected to the electrical motor and gearhead. This is a non-optimal solution because although miniaturized, the transmission is back-drivable and thus the motor gear head is exposed to shocks. In this paper we present the design of a non-back-drivable rotary mechanism with intrinsic compliance for a robotic thumb ab/adduction joint. The mechanism enables to switch-off the power supply once a desired posture is stable, thus avoiding accidental dangerous releases of the grasped object, and absorbs the impact forces generated at the instant of grasping and dissipates the repeated strains that are induced during manipulation. The mechanism was developed and tested. Detailed kinematic, static and stiffness analyses are presented as well as experimental measurements which demonstrate suitable performance for our application (max efficiency ~0.85, critical load 1.2 Nm, energy absorbed 1.5J).

Keywords: Non-back drivable, Compliant mechanism, Robot hand, shock absorber, Thumb abduction

Introduction

The performance of a robotic hand strongly relies on the choice of the actuation and transmission systems; the latter will determine to a large extent the energy consumption, the available grip force, the weight and aesthetic factors like noise and size [1]. The two key features that make a mechanical transmission suitable for anthropomorphic robotic hands are miniaturization and robustness [2]. Miniaturization is necessary in order to fit all functional parts (mechanisms, sensors, electronic controller) within the volume of a human-sized hand. However the reduction in size of the components affects the strength of the transmission, i.e. miniaturization and robustness are strongly tied. Therefore, if

miniaturization and robustness are required, it becomes crucial to protect the critical parts from possible shocks and overloads that might occur during operation. A compliant mechanism is one of the solutions that can effectively address shocks and overloads issues. Indeed, the presence of passive compliance within the hand actuators can (i) absorb the impact forces generated at the instant of grasping, (ii) dissipate the repeated strains that are induced during manipulation, (iii) adjust the backlash of the mechanism and, not less important, (iv) endow the hand with a biomimetic human-like stiffness when interacting with humans [3].

Another effective way to ensure a longer life to a mechanical component is to disengage the transmission whenever the load comes from the output drive. This is possible by means of a non-back drivable mechanism: a system in which the motion is transmitted only from the input to the output axis and not vice-versa. In a robotic hand such property enables to switch off the power supply, once a desired posture or grasp has become stable [4][5][6]. In grippers or hands employed as end effectors in humanoid or industrial robots, non-back-drivability is important for safety reasons: a power supply failure should not cause a possibly dangerous release of a grasped object or tool due to back-drivable transmissions. Moreover in grippers with high level of underactuation, the existence of a minimum number of non-back-drivable mechanisms is mandatory in order to produce first order form closure grasps [7]. However, conventional miniaturized non-back-drivable mechanisms (like lead screw pairs, worm gear pairs or gearheads with large reduction ratios) are generally energetically inefficient [4], thus not always desirable.

In humans, the thumb plays a unique role in the function of the hand, being essential for the formation of the pollici-digital pincers (opposition movements) and for the development of a powerful grip along with the other fingers. Due to the thumb, the

human hand is able to perform both power and precision grasps, achieving high dexterity and versatility [8]. Anatomically, the thumb has five Degrees of Freedom (DoF) in three joints inserted by 5 muscles. The thumb articulations are more exposed to accidental bumps and overloads partly due to its role of opposing the other fingers and partly due to its location anterior to the palm and the other fingers (which makes it more exposed in the environment). Statistics about injuries demonstrate this [9][10]. For the reasons described above duplicating the complexity of the human thumb with a robotic one is a very difficult task for engineers, taking into consideration the miniaturization and robustness requirements. The common way for addressing this problem was by simplifying the articulation.

In literature there are several examples of dexterous (but simplified) thumbs: Dechev et al. [11] designed a two DoFs thumb with actuated flexion/extension and passive ab/adduction. More recently other hands were provided with 2 DoFs actuated thumbs; Pons et al. [1] used a thumb in which ab/adduction and flexion/extension were coupled by means of a Geneva wheel. Cipriani et al. [12] and Butterfass et al. [13] designed thumbs with independently actuated ab/adduction and flexion/extension. Similarly commercial prosthetic hands like the i-Limb pulse (Touch Bionics Inc., Livingstone, Scotland) and Be-Bionic 3 (RSL Steeper ltd., Leeds, England) presented two DoFs thumbs with an actuated flexion/extension and a passive (manual) abduction/adduction. Notably, although not self-contained, the thumb of the DLR arm represents an interesting solution [15]: Grabenstein et al. developed a 3 DoFs thumb in which flexion/extension and ab/adduction movements were independently actuated by means of a robust bio-inspired actuation system based on antagonistic elastic tendons.

Most frequently the ab/adduction DoF consisted of a direct and rigid connection between the actuator (usually an electrical motor with integrated gearhead) and the axis

of the joint [1][12][13]. These transmissions were back-drivable so that all the external forces/perturbations applied on the thumb were rigidly transmitted to the miniaturized (thus fragile) gearhead of the actuator. As a result these mechanisms were neither particularly robust, nor particularly safe in the case of electrical power failure.

In this work we present a new, miniaturized, compliant and non-back-drivable mechanism for the ab/adduction DoF of a robotic thumb that can increase the robustness of the hand and the grasp safety. The mechanism is based on an efficient clutch coupled with a module endowed with non-linear mechanical compliance. It was specifically designed in order to be placed between the actuator (a miniaturized motor with integrated gearhead) and the ab/adduction joint of the IH2 Azzurra robotic hand i.e. the commercially available hand described by Cipriani et al., [12] (Prensilia Srl, Pisa, Italy). The clutch is an optimized version of the one proposed by Controzzi et al., [4], which exhibited small backlash, high efficiency and sustained a large Critical Load (CL, defined as the external, output torque that makes the system temporarily back-drivable). In this new version, the physical parameters that affected the CL of the system, were analysed in detail, in order to optimize the design. The new clutch was specifically designed for a thumb ab/adduction mechanism and compliant features were included.

Mechanism and architecture

The mechanism (Figure 1) is composed of a clutch, i.e. a Non-Back Drivable Mechanism (NBDM, Figure 1-b) in series with a Compliant Module (CM, Figure 1-c). The NBDM is based on a well-known mechanism (the two-way roller clutch), already proposed and designed by the authors for generic robotic applications [4]. The new design was optimized for reliability and exploitation in the abduction/adduction joint of a robotic thumb. The NBDM is composed of a fixed ring (1 in Figure 1) secured to the

ground (e.g. the frame of the hand), an input shaft and carrier plate (2) shaped with a three tooth extrusion ($2/_1$) and a coaxial key, a cam ($3/_1$) coaxial with the input shaft and mating keyway, fixed to the output shaft (3), six rollers (4, 5) which, under the action of six compression springs (6), tend to wedge between the fixed ring (1) and the cam ($3/_1$). When the input shaft is rotated clockwise/counter-clockwise the tooth extrusions ($2/_1$) unlock the rollers (5, 4) and the key transmits torque to the output shaft through the key/keyway connection. The transmission from the output shaft to the input shaft is not allowed, because the rollers [(5) or (4)] block the rotation of the cam and thus the keyway cannot make contact with the key. Compared to our previous version [4] this new system was improved because (i) all components were designed with the aim of reducing the manufacturing costs and simplifying the assembly procedure; (ii) three pairs of rollers were used (instead of two) in order to enhance the stability of the mechanism (alignment of the key/keyway connection), so to increase the critical load (CL) of the system and to reduce contact pressures.

The CM is mounted in series with the NBDM (Figure 1) in a way that the output shaft of the NBDM (3) corresponds to the input shaft of the CM. The CM is basically a cross-shaped key/keyway connection ($3/_2$) with embedded elastic materials (7) (Figure 1-c). The torque is transmitted from the input (3) to the output (8) and vice-versa, by means of four elastic inserts made of polymeric material (7) compressed within the keyway. The stiffness response is non-linear with respect to the compression of the elastic inserts. For small compressions (i.e. small rotations) the stiffness is low; for larger compressions the stiffness increases. Four rigid pins (9) embedded into the polymeric inserts limit their compression mechanically and make their stiffness virtually infinite. The maximum input-output angular shift of the CM is thus set by the length of these pins.

When the thumb ab/adduction DoF is actuated through the NBDM by means of a driving torque τ_i., there is a direct transmission between the input drive and the thumb ab/adduction, as long as the output torque (τ_o) is below τ_i. When the input drive stops the thumb keeps the reached position without consuming power, due to the NBDM. Eventual gears and/or mechanisms (in general a transmission, like a motor gearhead) connected to the input drive of the NBDM are protected against overloads (when $\tau_o <$ CL) by the NBDM itself. External loads applied to the thumb are transmitted to the mechanism and eventually to the frame. In all cases the CM dampens impulsive torques that could potentially overcome the CL of the NBDM and thus make the system back-drivable.

System Analysis

The system was specifically designed for robotic hands. Kinematic, static and stiffness analyses were performed and are described in the following paragraphs.

Kinematic analysis of the NBDM

Backlash is always a critical aspect in mechanical systems. In dexterous robotic hands this issue is even more important with respect to manipulation tasks [16]. For this reason a kinematic analysis of the NBDM was conducted in order to minimize its backlash. This implies a critical analysis of the inner clearances, micro-mechanics manufacturing processes and working principles of the mechanism. In the proposed mechanism, theoretically, the output backlash is zero due to the action of the springs that wedge the rollers between the ring and the cam. At the other side, at the input, a minimum backlash is unavoidable because a minimum clearance is required in order to unlock the rollers only when desired, i.e. when the unlocking condition is met. This specific condition is graphically described in Figure 2. The input shaft must first rotate

by an angle g_1 (Figure 2-b) in order to contact and unlock the rollers and then, when it is further rotated by an angle g_2 (with $g_2 > g_1$) (Figure 2-c), it starts dragging the cam and transmits torque to the output. The angle g_2 is the actual backlash of the NBDM and corresponds to the angle between the lateral surface of the input shaft key and the keyway on the cam. Although the architecture of the present NBDM is slightly different from our previous design [4], the same kinematic analysis applies.

Static analysis of NBDM

When an external torque is applied to the output of the NBDM, the system is locked due to the three rollers which are wedged between the ring and the cam, as represented in Figure 3-b. This is true when two conditions are met: i) the roller-cam and the roller-ring frictions are large enough to maintain the rollers wedged; ii) there is a gap between the roller and the unlocking tooth (defined as Unlocking Gap, UG) (Figure 3-a). The UG is required in order to unlock the system only when tangible forward motions are involved (and is the reason for the input backlash). A static analysis of the system was conducted in order to correctly tune the design parameters that comply with these two conditions.

Figure 3-c shows the roller/cam and roller/ring interaction forces when an external torque τ_o is applied from the output (i.e. to the cam shaft). In this case each roller is under the action of the forces F_{RC} (between the roller and the cam) and F_{RR} (between the roller and the ring), calculated as:

$$F_{RR} = F_{RC} \qquad (3)$$

$$F_{RC} = \frac{\tau_o}{3b} \qquad (4)$$

where b is the lever arm of F_{RC} and 3 is the number of rollers engaged. The radial (R) and (T) tangential components of F_{RC} can be calculated as follows:

$$R_{RC} = F_{RC} \cos \alpha = \frac{\tau_o cos\alpha}{3b} \quad (5)$$

$$T_{RC} = F_{RC} \sin \alpha = \frac{\tau_o \sin \alpha}{3b} \quad (6)$$

with α the angle between the axis crossing the two contact points (between the roller and cam/ring) and the axis connecting each contact point to the center of the roller. In other words, α is an index of how parallel the ring and cam surfaces are: when $\alpha = 0$, the ring and the cam are parallel. The radial and tangential components are thus proportional to the external torque τ_o.

The locking condition is met when the tangential force T_{RC} is lower than the friction:

$$T_{RC} < R_{RC}\mu_s \rightarrow \frac{\tau_o \sin \alpha}{3b} < \frac{\tau_o \cos \alpha}{3b} \mu_s \rightarrow \mu_s > \tan \alpha \quad (7)$$

where μ_s is the static friction coefficient between the rollers and the ring and between the rollers and the cam.

In conclusion, the locking condition depends on the static friction coefficient μ_s and on the geometric angle α. Hence, the choice of α is a key issue for the design of the cam profile. In particular α should be a trade-off between two opposite requirements: i) $\tan \alpha$ must be lower than μ_s in order to allow the locking condition [Equation (7)], however, ii) if α is too small, the mechanism is more prone to unlock for very small deformations of the rollers, because the UG reduces (as the roller can get closer to the tooth). The reduction of the UG (ΔUG) and the reduction of the diameter of the rollers (Δd) are ruled by the following equation:

$$\Delta UG = \frac{\Delta d}{2 \sin \alpha} \qquad (8)$$

These opposite requirements ruled by α are graphically described in Figure 4. Equation (7) is in blue dotted line; equation (8) (in blue solid line) is plotted with a fixed Δd (equal to 0.1 mm - a wear and/or deformation value that is unlikely to be reached in the practice). The graph shows (in the white window) the angular range allowed to α (which must be within the two limits α_{max} and α_{min}) in order to permit the locking of the mechanism. The upper limit (α_{max}) is set by the locking condition ruled by equation (7). The lower limit (α_{min}) depends on the input backlash allowed by the design. In the graph α_{min} corresponds to the angle reached when the ΔUG is equal to UG* (maximum unlocking gap permitted, as defined by the design requirements). In our specific design a UG* equal to 0.6 mm corresponded to an input backlash of 6° deg. In the graph an α equal to 9° deg (red line in Figure 4) insures an equal safety margin between α_{max} and α_{min} (considering steel-brass coupling between rollers and the other parts).

When α is included between α_{max} and α_{min} the system unlocks only if τ_o reaches the CL value, i.e. if τ_o is large enough to generate large plastic deformations in the contact areas between the rollers and the other components. Indeed when plastic deformations occur the static friction coefficient decreases linearly with the increasing of τ_o until the unlocking condition is met [14].

Stiffness analysis of the Compliant Mechanism

The CM was designed as a cross-shaped key/keyway connection with embedded inserts made of polymeric material. The optimal combination of shape and material was chosen aided by a Finite Element Analysis (FEA) (Ansys Inc., Cecil Township, Pennsylvania, USA) performed for evaluating the characteristic of the CM under external loads. The model predicted the characteristic of the CM (torque τ vs. rotation angle of the output

shaft γ) which is a function of several parameters and could be easily adjusted by design. For example, by increasing the preload of the deformable inserts (by manufacturing inserts larger than their housings) the CM could exhibit a larger stiffness offset, whereas by varying the material different stiffness could be achieved.

Design requirements, material selection and development

The presented mechanism was designed using CAD tools in order to miniaturize its size and weight for integration in the IH2 Azzurra robotic hand (Prensilia Srl, Pisa, Italy). In particular, the maximum diameter allowed (i.e. 24 mm) was constrained by the thickness of the palm, while the maximum length allowed (i.e. 33 mm) was constrained by the gap between the motor shaft (Faulhaber 1316, gearhead 14/1, ratio 246:1) and the edge of the hand. Some space was also necessary in order to fit a suitable transmission between the mechanism and the ab/adduction joint of the thumb. In addition to volumetric constraints there were robustness requirements: the thumb of the hand was required to sustain at most a 3.5 kg object using a palmar power grasp (those that engage the palmar areas of the hand), corresponding to a torque of ~600 Nmm on the ab/adduction joint. The NBDM and the CM were designed considering these requirements. The pictures in Figure 5 show one of the manufactured prototypes also integrated in the robotic hand. The picture also shows the compact transmission based on bevel gears chosen to connect to the joint of the thumb. The volume of the whole mechanism (NBDM+CM) is about 5500 mm^3 (including the 31 mm long shaft; maximum diameter: 23 mm) and the weight is 32 g. In particular, the volume of NBDM is about 4000 mm^3 and the weight is 23 g: the dimensions were reduced by roughly 25% with respect to our previous prototype [4].

Non back drivable mechanism

Critical parts of the mechanism [cf. Figure 1 - fixed ring ($1/_1$), input shaft (2), cam (3), and carrier plate ($2/_1$)] were manufactured using stainless steel (AISI 316 series). Stainless steel allows to transmit torque stresses, resists to surface stresses induced by the wedging of the rollers and resists to lubricant corrosion. The rollers were manufactured using brass (frictionless alloy) as it demonstrates good proprieties in terms of: friction, mechanical resistance, superficial hardness, resistance to corrosion and thermal stability. All of these properties are mandatory for rollers that must rotate and wedge between hard surfaces. The NBDM was designed with an angle α of 9° deg, based on equations (7, 8) and on the steel-brass friction coefficient ($\mu_s = 0{,}25$) (cf. Figure 5). Ergal aluminum alloy (7075 series) was chosen for those parts not subjected to high stresses and plain bearings were used to support the input/output shafts (instead of ball bearings, in order to miniaturize the mechanism). The compression springs in the NBDM were commercially available (model: D10210, MeterSprings Srl, Biella, Italy). The system was designed with an input backlash of 6 degrees, based on the manufacturing facilities available at our lab.

Compliant mechanism

The stiffness of the thumb ab/adduction DoF is an important design issue. If the joint is too much compliant the fingertip might be too loose and thus its position be affected by the effects of the weight and inertia of the thumb and of the grasped object. In fact if the thumb is grasping an object in a thumb-index or a thumb-index-middle grip (the so called *precision grips* prehensile forms [17][18]) a loose ab/adduction joint might cause losses of the grasp stability due to the object weight and inertia (while moving). Hence the position of the fingertip and so the posture of the hand could become unobservable

and even worse, the hand might be unable to perform stable precision grips. Conversely, a too stiff CM is not desirable because all the advantages of having a compliant DoF would be lost. In short a trade-off is necessary. We based our design on the following two needs.

(1) The thumb should be able to hold the heaviest object allowed (i.e. 3.5 kg, corresponding to a torque of ~600 Nmm on the ab/adduction joint) in palmar power grasps, with limited displacement of the thumb (10 mm at the tip, corresponding to 5° deg). Larger displacements of the fingertip would result in unstable grasps.
(2) The input drive of the CM (i.e. the NBDM and the motor gearhead) should be protected from overloads and shocks.

Different elastomeric materials were investigated for molding the elastic inserts of the CM, in order to find the optimal solution. The response of a urethane rubber, shore A75 (PMC dry, Smooth On Inc., Easton PA, USA) was found the most compatible with our requirements. Stainless steel (AISI 316 series) was selected for the output of the CM [(8) in Figure 1], since this component is subjected to high stresses. The external ring of the CM [component ($1/_2$)] serves as a plain bearing and thus was made in brass. Ergal aluminum alloy (7075 series) was chosen for the other, non-critical parts. The maximum angular displacement was set to 5° deg by trimming the length of the rigid pins (9).

Experimental Results

Experimental measurements were performed on the developed prototypes in order to evaluate: i) the efficiency and ii) the critical load of the NBDM, iii) the response of the elastomeric inserts of the CM vs. the FEA simulations, iv) the protection offered by the

CM to a fatigue test and v) to shocks.

Efficiency

The set-up shown in Figure 6-a was used to experimentally measure the efficiency of the NBDM and of the whole mechanism (NDBM+CM). In the first case, the DUT (Device Under Test) was the NBDM, which was connected to the motor shaft of an electrical DC motor (Faulhaber 1316 SR, gearhead 14/1, ratio 246:1). Electrical current and rotation speed were measured varying the motor voltage in steps of 1 V, with no load conditions. Same measurements collected on the motor alone, permitted to derive the efficiency of the NBDM (as in [4]), which is plotted in Figure 7 (blue curve). In the operative speed of 3÷4 rad/sec (corresponding to an abduction time of 0.6÷0.4 second) the efficiency of the NBDM was greater than 70 %. Equivalent measurements with the DUT being the NBDM and CM combined, demonstrated an efficiency reduced by ~15% in the whole range (Figure 7, red curve).

Critical Load of the NBDM

The setup for measuring the CL is graphically depicted in Figure 6-b; in this case the NBDM was the DUT. The output of the NBDM was connected to a pulley and a steel cable (2 mm diameter, inextensible in the range of force used, max load 2500N) in turn connected to the Instron tensile tester (Instron, Illinois Tool Works Inc., USA). The tensile tester was used to force the output of the NBDM (i.e. to rotate it until back-drivability was achieved) both clockwise and anticlockwise; meanwhile the reaction force was recorded. The CL experimentally determined as the average of 20 measures corresponded to a torque of ~1200 ± 50 Nmm (mean ± standard deviation). This value was two times larger than the minimum required by the design requirements. A slight reduction of the actual CL was observed trial after trial (3% maximum deviation from

the initial measurement). This reduction was caused by the plastic deformations of the rollers that occurred in consecutive CL conditions (cf. Paragraph 3.2), as confirmed by visually inspecting the rollers. In the present application this should not be an issue as lower loads (than those involved in these tests) are expected during the normal operation of the mechanism (which is also protected by the CM).

Stiffness

The stiffness of the CM was measured using the experimental setup shown in Figure 6-b, with the CM as the DUT. Although the material chosen for the elastic inserts in our application was urethane rubber, force/displacement measurements were performed both using urethane rubber and soft silicone shore 00-30 (EcoFlex, Smooth On, Smooth On Inc., Easton PA, USA), in order to assess the validity of the FEA model. The graph in Figure 8 shows the torque (τ) versus the angular displacement (γ) computed by the FEA and experimentally measured (urethane rubber in blue; soft silicone in green; bold lines refer to the FEA). The average relative errors between the FEA model and the experimental measurements were small: 6,4 % for the urethane and 1,6% for the soft silicone.

The CM with urethane inserts showed a close-to-constant torque/rotation relationship and a maximum torque of ~600 Nmm for a 5° deg rotation. With inserts molded in EcoFlex30 the CM showed a more non-linear characteristic, thus showing how the latter depends on the shore of the inserts.

Fatigue test

Cyclic loading torques were applied to the output of the CM using the Instron tensile tester (Figure 6-c). One test specimen (ergal aluminum alloy, breaking torque: 900

Nmm) was connected between the input shaft of the CM (where the ab/adduction motor would be placed) and a fixed frame. Cyclic angular rotations (γ_F) (with fixed rotation angle and almost static conditions) were applied to the test specimen through the CM. When the test specimen broke (due to low cycle fatigue [20]), the test ended and the number of cycles (i.e. the *fatigue life, N_F*) was noted down. This test was performed both using the CM (urethane inserts) and without it. In the second case, the test specimen was directly connected to the machine (and served as the control condition).

The fatigue life for 20 test specimens at different angles (γ_F = 15°, 10°, 8.5°, 7°, 5° deg with the CM and γ_F = 10°, 5°, 3°, 2° deg without CM) is plotted in Figure 9 (N_F, in red with the CM, in blue without the CM). The use of the CM increased the fatigue life by roughly one order of magnitude. When the rotation angle was lower than 8.5° deg (7° and 5°) it was impossible to break the test specimens within 10'000 cycles (after 10'000 cycles the test was aborted).

Impulsive load test of the CM

The ability of the CM to absorb impulsive loads was evaluated as follows: the output of the CM was rigidly connected to an aluminum bar (80mm length, like a robot thumb). The input of the CM was connected to a test specimen grounded to a frame. A 1 Kg mass was dropped from a specific height in free air at a specific moment arm on the bar (Figure 6-d). The height was reduced in steps of 3 cm. The minimum height at which the test specimen did not break was used to calculate the absorbed energy. This corresponded to 1.5 J with the CM and 0.9 J without it (bar directly attached to the test specimen). Thus, the CM incremented the energy absorbed by more than 60%.

Together, the fatigue test and the impulsive load test demonstrated how the CM can protect a transmission and be effective in preventing failures when slow-phased or

sudden mechanical disturbances (within certain amplitude levels) occur.

Discussion

The low efficiency of the mechanism, when the CM is included is mainly caused by the friction between the ring [($1/_2$) in Figure 1] and the output shaft (8) (this connection works as a plain bearing). In the operational range the measured efficiency can be deemed acceptable for our application; it could be sensibly reduced by replacing all the plain bearings with roller bearings at the expense of miniaturized dimensions of the mechanism.

The CL of the NBDM is strongly affected by the diameter, shape and material of the rollers. As already discussed in [4], the choice of these design parameters was made in order to find the best trade-off between efficiency, CL and overall dimensions. A CL of 1.2 Nm was achieved with brass rollers, particularly suitable for our application. The CL could be increased using steel rollers (with a Young's module larger than brass); however, since the friction coefficient using steel rollers would be higher, the efficiency of the mechanism would be reduced.

Elastomers are of particular interest for the present application because of their non-linear stiffness that makes them more similar to biological springs than traditional steel springs [14]. This is obviously an important feature for a joint in an artificial hand, expected to mimic human movements and to fluently interact with individuals. Considering the miniaturization of the proposed system, it would be extremely challenging to manufacture steel springs with similar characteristics and costs. However for those applications where size is not an issue steel springs could be a viable solution.

The elastic inserts were made in urethane rubber, based on the requirements of our

application. However, in a different application softer polymers could be used; this would increase the resistance to impulsive loads and to cyclic deformations, at the expense of a reduced positioning accuracy of the end point.

Conclusions

In this work we presented the design, development and experimental assessment of a compact a non-back-drivable mechanism with intrinsic compliance suitable for the ab/adduction joint of a robotic thumb. The development of such joint is one of the most challenging technical tasks when designing artificial anthropomorphic hands. In fact its role while grasping and its position in the hand make the thumb more exposed to accidental bumps and overloads than the long fingers.

Our design included a non-back-drivable mechanism (NBDM) and a compliant mechanism (CM). The NBDM was used to prevent losses of grasp stability in the case of electrical power failure, and to protect the input drive from external loads. The CM was designed for absorbing the impact forces generated at the instant of grasping, and among the others, for endowing the hand with a biomimetic human-like stiffness when interacting with humans. Prototypes were developed and tested; the volume of the whole mechanism (NBDM+CM) was about 5500 mm^3 and the weight was 32 g. Experimental measures demonstrated a maximum efficiency of ~0.85, a critical load of 1.2 Nm, and a capacity of absorbing energy of 1.5J. The mechanism was purposely designed for the ab/adduction joint of a specific robot hand, however, the design could be exploited in a wide range of robotic applications where a safe, miniaturized, low-cost, high efficiency and compliant actuation unit is required.

Acknowledgments

Authors would like to thank Nicodemo Funaro for his precious work.

Funding

This work was supported in part by the European Commission under the COGLABORATION project (EU-FP7-ICT-287888) and by the Italian Ministry of Education University and Research, under the FIRB-2010 MY-HAND Project [RBFR10VCLD].

Nomenclature

DoF	Degree of freedom
CL	Critical load
NBDM	Non back drivable mechanism
CM	Compliant mechanism
FEA	Finite element analysis
CAD	Computer aided design
DUT	Device under test
UG	Unlocking gap
Δd	Variation of the diameter of the roller
τ_o	Torque applied at the joint output
τ_i	Input torque
g_1	Unlocking angle
g_2	Input backlash angle
F_{RC}	Contact force between the roller and the cam
F_{RR}	Contact force between the roller and the ring
R_{RC}	Radial component of F_{RC}
T_{RC}	Tangential component of F_{RC}
α	Angle between the axis crossing the two contact points and the axis connecting each contact point to the center of the roller

μ_S	Static friction coefficient
γ	Rotational angle of the output shaft of the CM
N_F	Fatigue life
γ_F	Cyclic angular rotation in the fatigue test of the CM

References

[1] Pons, J.L., Rocon, E., Ceres, R., Reynaerts, D., Saro, B., Levin, S. and Van Moorleghem, W., 2004, "The MANUS-HAND dextrous robotics upper limb prosthesis: mechanical and manipulation aspects", Autonomous Robots, **16**(2), pp. 143-163.

[2] Controzzi, M. Cipriani, C., Carrozza, M.C., 2014, "Design of artificial hands: a review". in *The Human Hand: A Source of Inspiration for Robotic Hands*, Springer Tracts in Advanced Robotics (STAR) series, Balasubramanian, R. and Santos, V.J., Eds., Springer, Heidelberg, 95, pp. 219-246.

[3] Albu-Schaffer, A., Eiberger, O., Grebenstein, M., Haddadin, S., Ott, T., Wimbock, C., Wolf, S., Hirzinger, G., 2008, "Soft robotics", IEEE Robotics & Automation Magazine, **15**(3), pp. 20-30.

[4] Controzzi, M., Cipriani, C. and Carrozza, M. C., 2010, "Miniaturized non-back-drivable mechanism for robotic applications", Mechanism and Machine Theory, **45**(10), pp. 1395-1406.

[5] SungKu, K., In, H., and Cho K.J., 2012, "Design of a passive brake mechanism for tendon driven devices" International Journal of Precision Engineering and Manufacturing, **13**(8), pp. 1487-1490.

[6] Koganezawa, K., 2010, "Back-drivable and Inherently Safe Mechanism for Artificial Finger", *Proceedings of Robotics: Science and Systems 2010*, Spain.

[7] Krut, S., Bégoc, V., Dombre, E. and Pierrot, F., 2010, "Extension of the form-closure property to underactuated hands", IEEE Transactions on Robotics, **26**(5), pp. 853-866.

[8] Kapandji, I. A., 1970, *The Physiology of the Joints, Upper Limb*, 2nd Ed. London: Livingstone, 1, pp. 182-201.

[9] Page, R.E., 1975, “Hand injuries at work: An analysis of patients attending hospital”, *The Hand*, **7**(1), pp. 51-55.

[10] Vadivelu, R., Dias, J., Burke, F. and Stanton, J., 2006, “Hand Injuries in Children: A Prospective Study”, Journal Of Pediatric Orthopaedics, **26**(1), pp. 29-35.

[11] Dechev, N., Cleghorn, W.L. and Naumann, S., 2001, “Multiple Finger, Passive Adaptive Grasp Prosthetic Hand”, Mechanism and Machine Theory, **36**, pp. 1157-1173.

[12] Cipriani, C., Controzzi, M. and Carrozza, M. C., 2011, “The SmartHand transradial prosthesis”, Journal of NeuroEngineering and Rehabilitation, **8**(29).

[13] Butterfass, J., Grebenstein, M., Liu H. and Hirzinger G., 2001, “DLR-Hand II: Next Generation of a Dextrous Robot Hand” *International Conference on Robotics and Automation ICRA 2001,* 1, pp. 109-114.

[14] Jones, J., 2000, *Contact Mechanics*, Cambridge University Press, Cambridge, UK.

[15] Grebenstein, M., Chalon, M., Hirzinger, G., Siegwart, R., 2010, “Antagonistically Driven Finger Design for the Anthropomorphic DLR Hand Arm System”, *IEEE-RAS International Conference on Humanoid Robots Nashville*, USA, pp. 609-616.

[16] Mason, M. T., & Salisbury Jr, J. K., 1985,. *Robot hands and the mechanics of manipulation,* MIT press, Cambridge, USA.

[17] Cutkosky, M. R., 1989, “On grasp choice, grasp models, and the design of hands for manufacturing tasks”, IEEE Transactions on Robotics and Automation, **5**(3), pp. 269-279.

[18] Iberall, T., Bingham, G., Arbib, M. A., 1986, “Opposition space as a structuring concept for the analysis of skilled hand movements”, In: H. Heuer, C. Fromm (eds.), *Experimental Brain Research Series 15 - Generation and Modulation of Action Patterns*, Springer-Verlag, pp. 158–173.

[19] Carter, R. R., Crago, P. E., Gorman, P. H., 1993, “Nonlinear stretch reflex interaction during co-contraction”, Journal of Neurophisiology, **69**(3), pp. 943-952.

[20] Juvinall R. C., Marshek K. M., 1991, *Fundamentals of Machine components design,* John Wiley & Sons. Inc., USA, Chap. 8.

Figure Captions List

Figure 1. Drawings of the mechanism proposed. (a) Exploded view of the mechanism. (b) Cross section of the NBDM (in grey) and of the CM (in white).

Figure 2. Drawings of the NBDM mechanism. (a) Neutral position. (b) Unlocking condition: the input shaft is rotated by an angle g_1. (c) Motion transmission condition: the input shaft is rotated by an angle g_2 which allows the key to make contact with the keyway. Angle g_2 corresponds to the input backlash.

Figure 3. Analysis of the NBDM. (a) Parametric scheme and cross section, where UG (Unlocking Gap) is the gap between the roller and the unlocking tooth and g_2 is the backlash of the NBDM and corresponds to the angle between the lateral surface of the input shaft key and the keyway on the cam. (b) Cross section of the locked mechanism; the rollers are wedged between the cam and the ring due to the external torque τ_O. (c) Static interaction forces among the cam-roller-ring components in the locked condition.

Figure 4. Static analysis chart of the NBDM.

Figure 5. Pictures of the developed mechanism. (a) Assembled mechanism. (b) Non Back Drivable Mechanism. (c) Compliant Mechanism. (d) Mechanism integrated in the IH2 Azzurra hand. The input of the NBDM is connected to a geared DC motor (Faulhaber 1316 SR, gearhead 14/1, ratio 246:1), while the output of the CM is connected to the thumb ab/adduction joint by means of two conic gears.

Figure 6. Experimental set-up of the different measures performed for evaluating the performance of the mechanism. (a) Efficiency test. (b) Critical Load of the NBDM and Stiffness characteristic of the CM. (c) Cyclic test. (d) Impulsive load test.

Figure 7. Efficiency of the NBDM and of the whole mechanism (NBDM+CM) vs. velocity and supply motor voltage.

Figure 8. Simulated (bold lines) and experimental (shadowed areas) characteristics (torque τ vs. angular shift γ) of the CM with urethane rubber inserts (blu curves) and soft silicone shore 00-30 (green curves). Dashed lines show the typical response during the relaxation phase of the test.

Figure 9. Fatigue life (N_F) versus cyclic loading angle (γ_F) of 20 test specimens (breaking torque: 900 Nmm) with (red circles) and without (blue squares) the CM. Bold lines describe the fitting of the measures. The vertical asymptote for γ_F =7° deg represents the fact that with the CM and 10'000 cycles the test-specimen did not break.

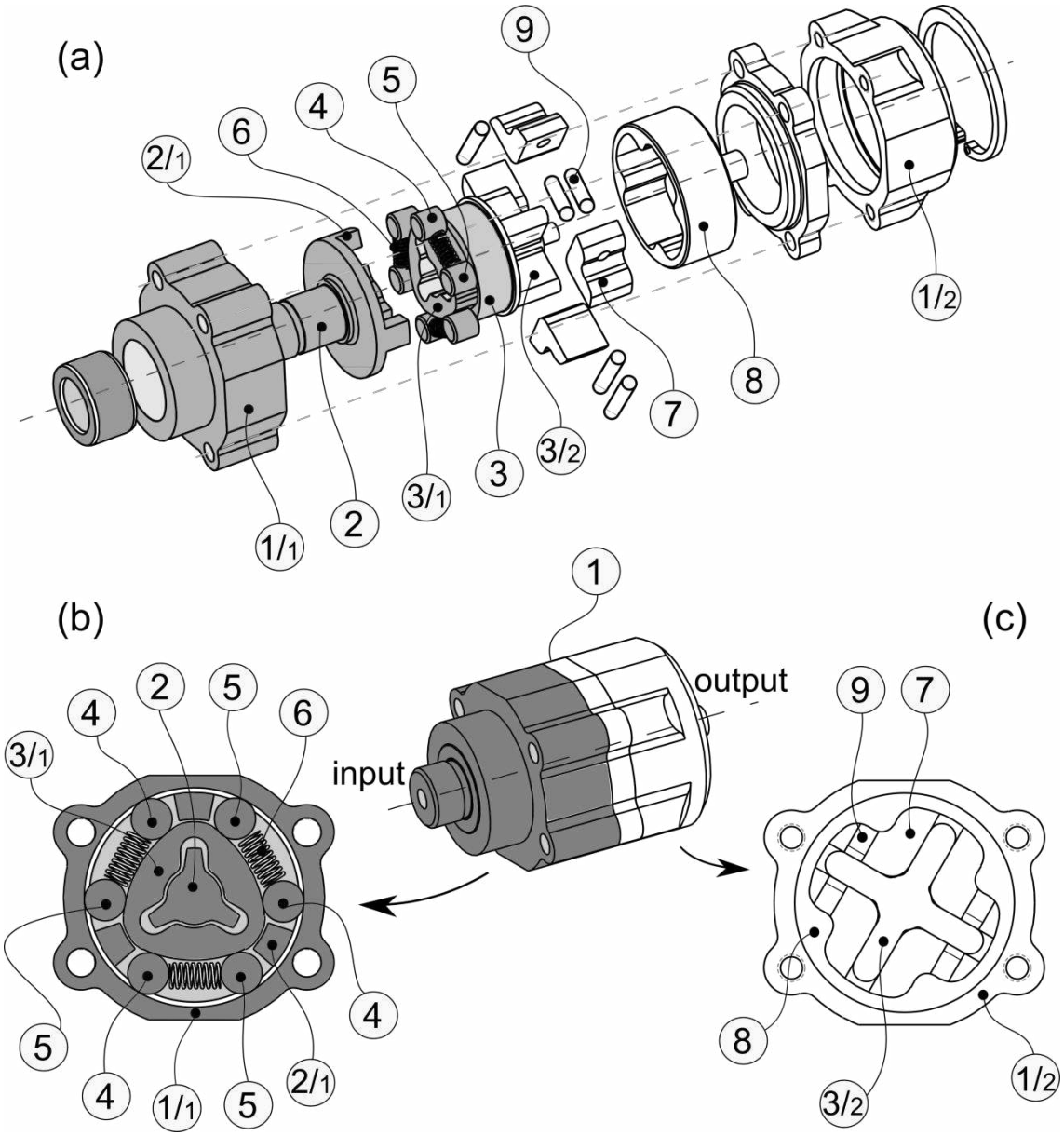
(a)
9
5
4
6
2/1
1/2
8
7
3/2
3
3/1
2
1/1
(b)
1
(c)
output
input
2
5
4
6
3/1
9
7
5
4
4
8
4
1/1
5
2/1
3/2
1/2

Figure 1

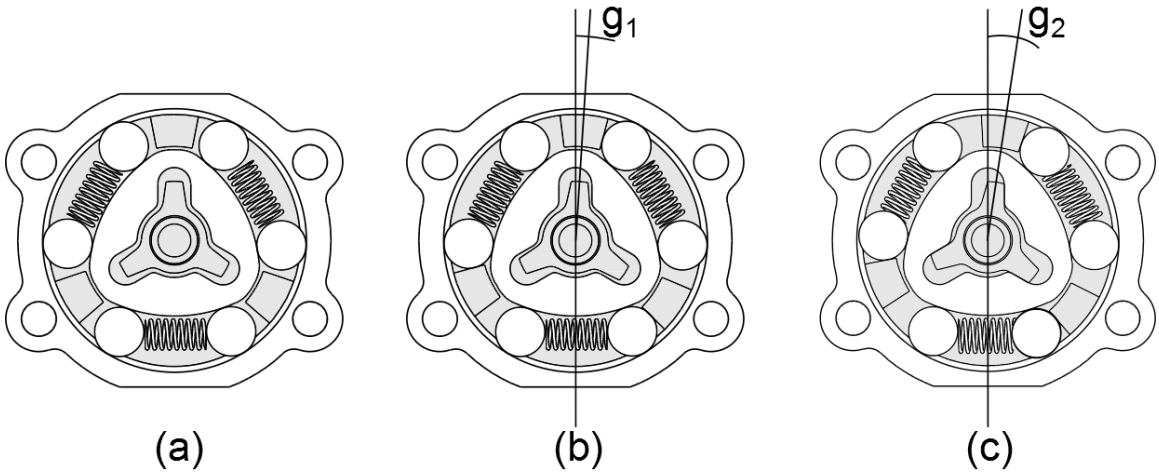

Figure 2

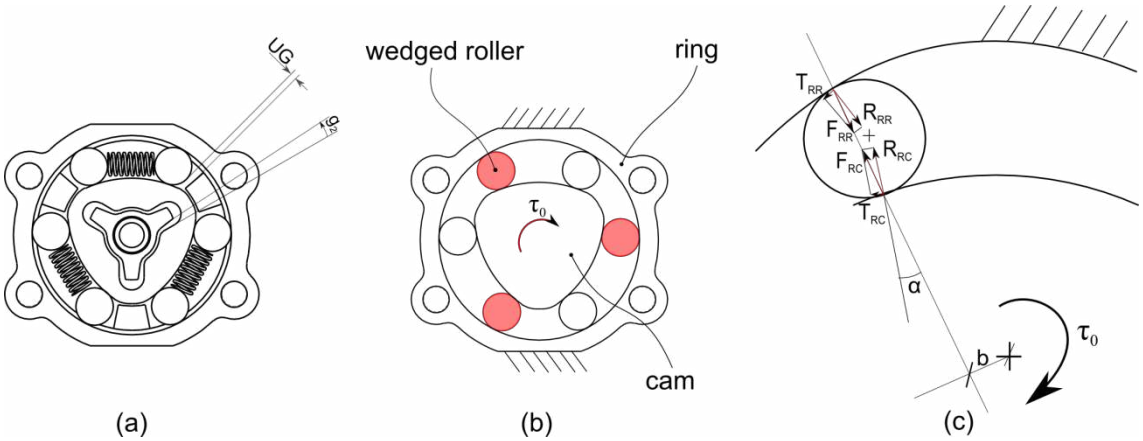
UG
wedged roller
ring
τ_0
cam
T_{RR}
R_{RR}
F_{RR}
F_{RC}
R_{RC}
T_{RC}
α
b
τ_0
(a)
(b)
(c)

Figure 3

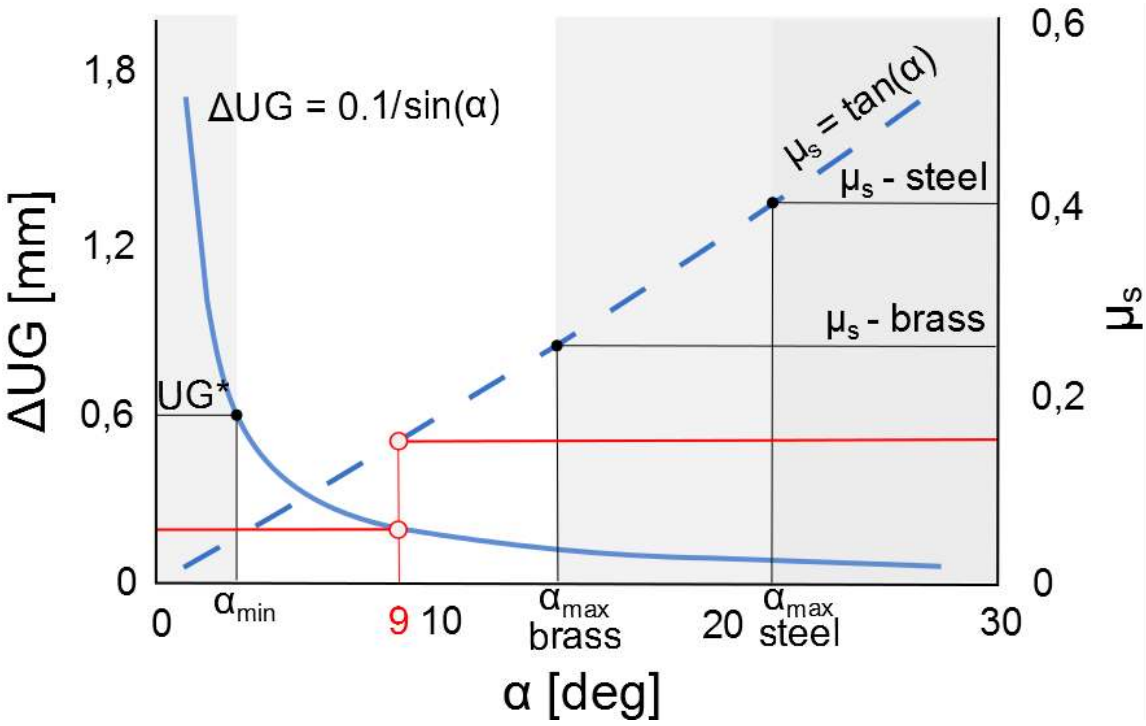
ΔUG [mm]
1,8
1,2
0,6
0
ΔUG = 0.1/sin(α)
UG*
μs = tan(α)
μs - steel
μs - brass
μs
0,6
0,4
0,2
0
0
αmin
9 10
αmax brass
20
αmax steel
30
α [deg]

Figure 4

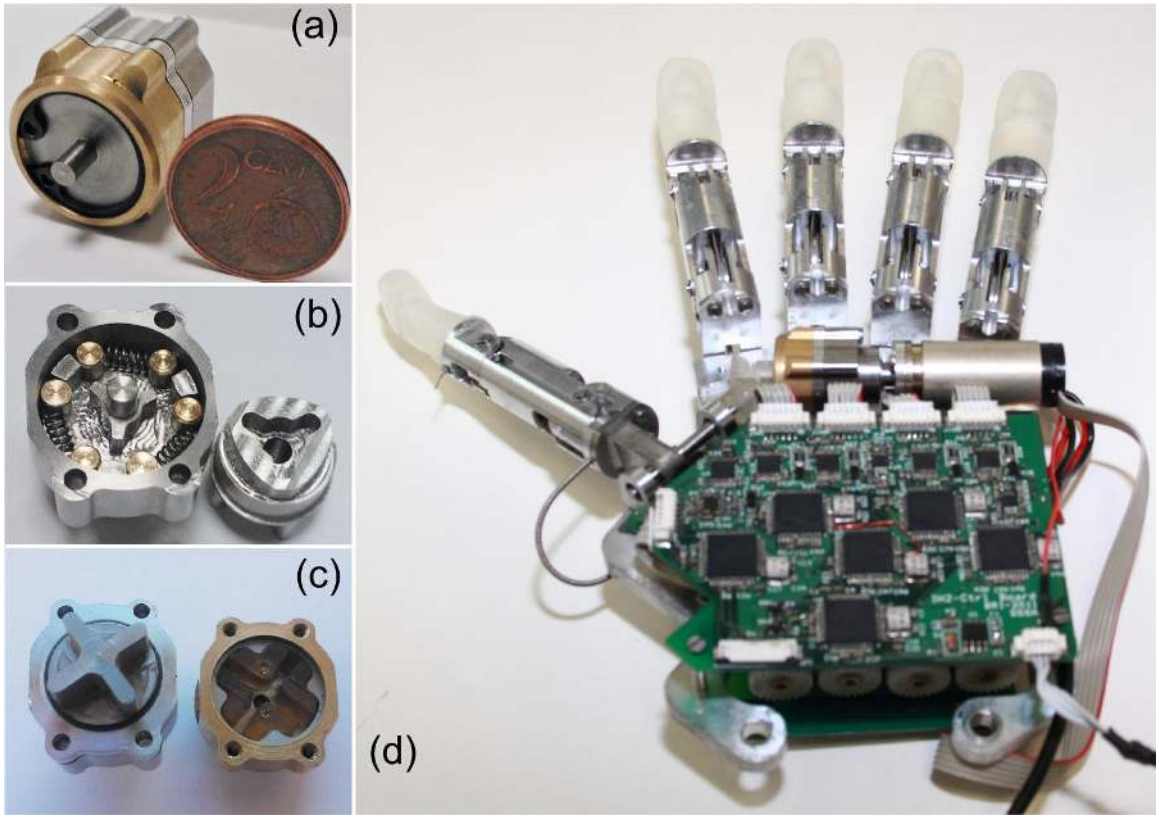

Figure 5

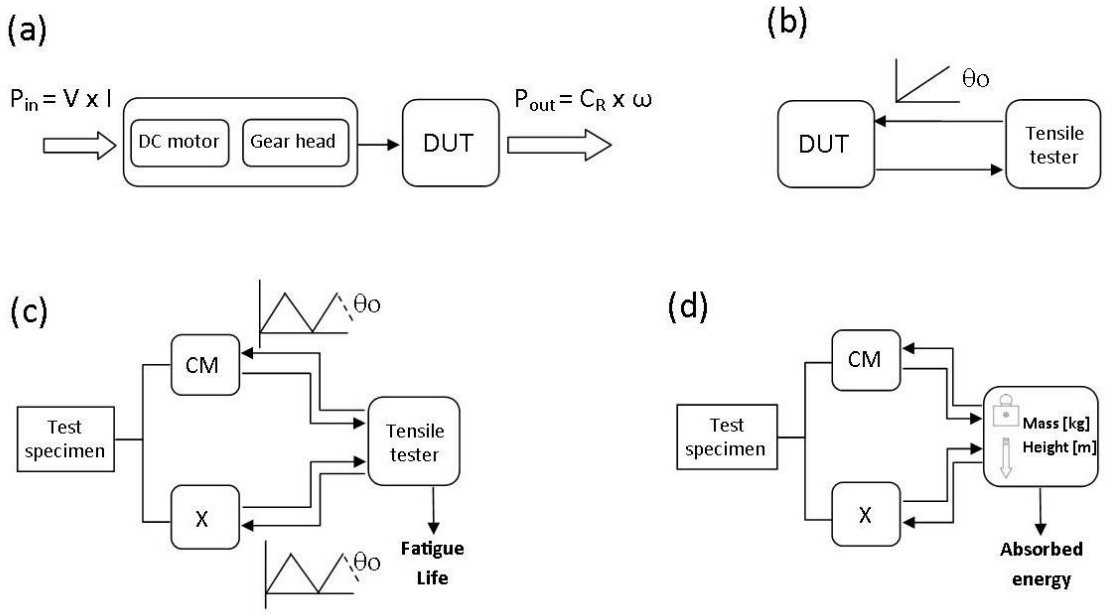
(a)
P_{in} = V x I
DC motor
Gear head
DUT
P_{out} = C_R x ω
(b)
θo
DUT
Tensile tester
(c)
θo
CM
Test specimen
Tensile tester
X
θo
Fatigue Life
(d)
CM
Test specimen
Mass [kg]
Height [m]
X
Absorbed energy

Figure 6

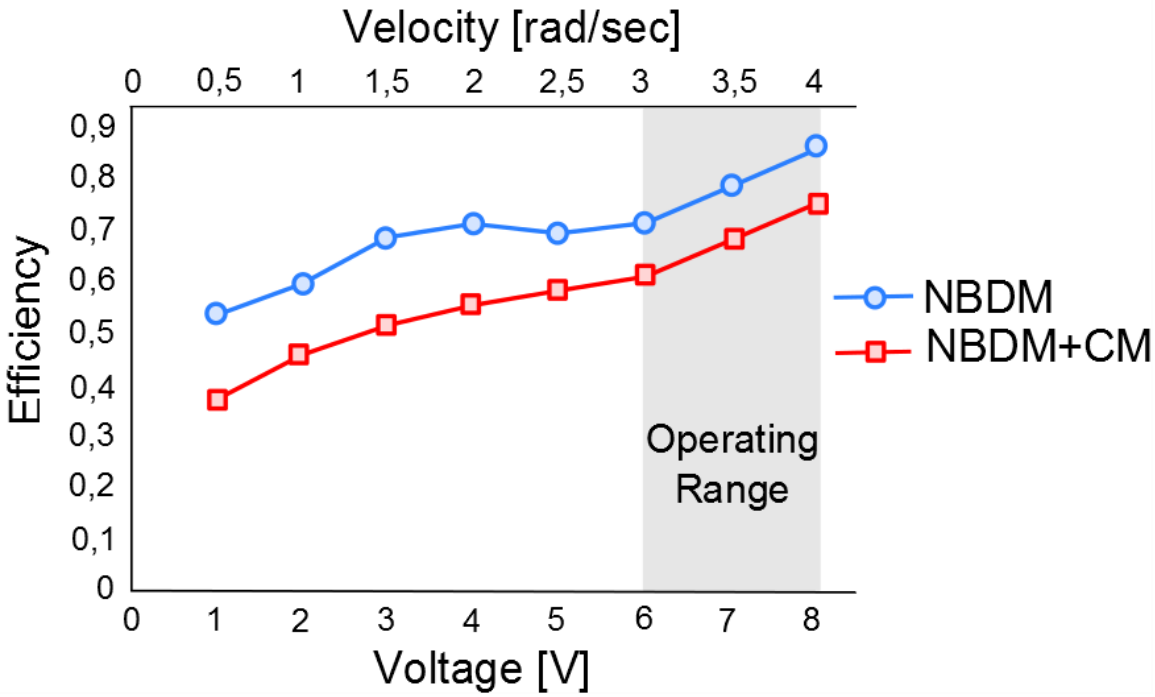
Velocity [rad/sec]
0
0,5
1
1,5
2
2,5
3
3,5
4
Efficiency
0,9
0,8
0,7
0,6
0,5
0,4
0,3
0,2
0,1
0
Operating
Range
NBDM
NBDM+CM
0
1
2
3
4
5
6
7
8
Voltage [V]

Figure 7

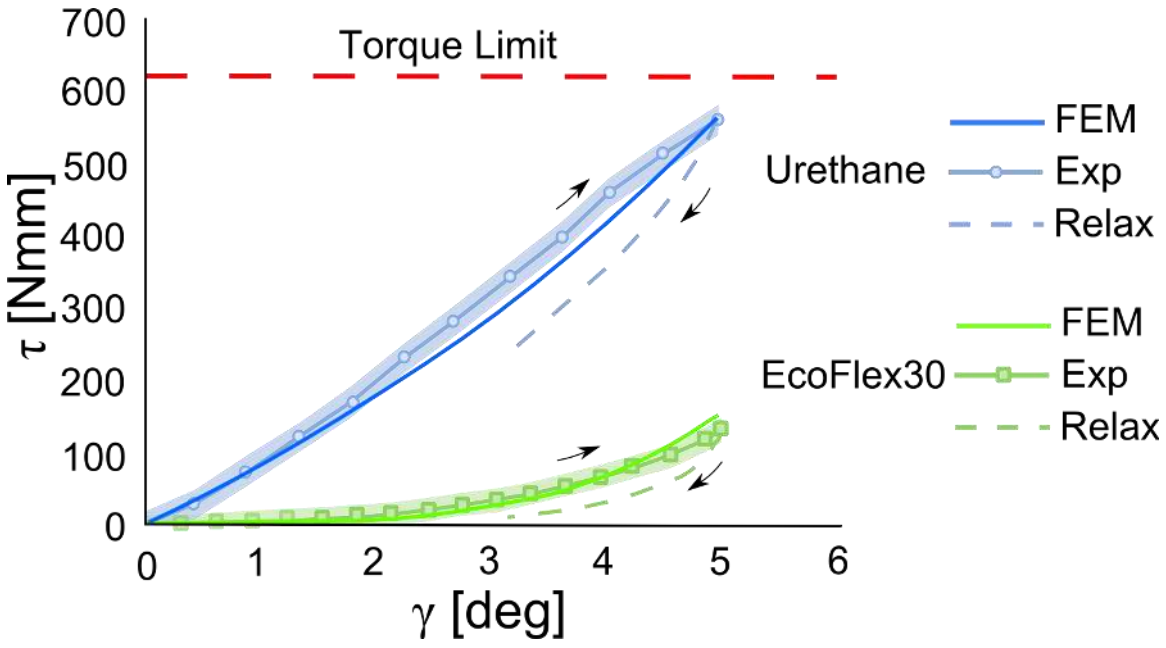
Torque Limit
700
600
500
400
300
200
100
0
τ [Nmm]
0
1
2
3
4
5
6
γ [deg]
Urethane
FEM
Exp
Relax
EcoFlex30
FEM
Exp
Relax

Figure 8

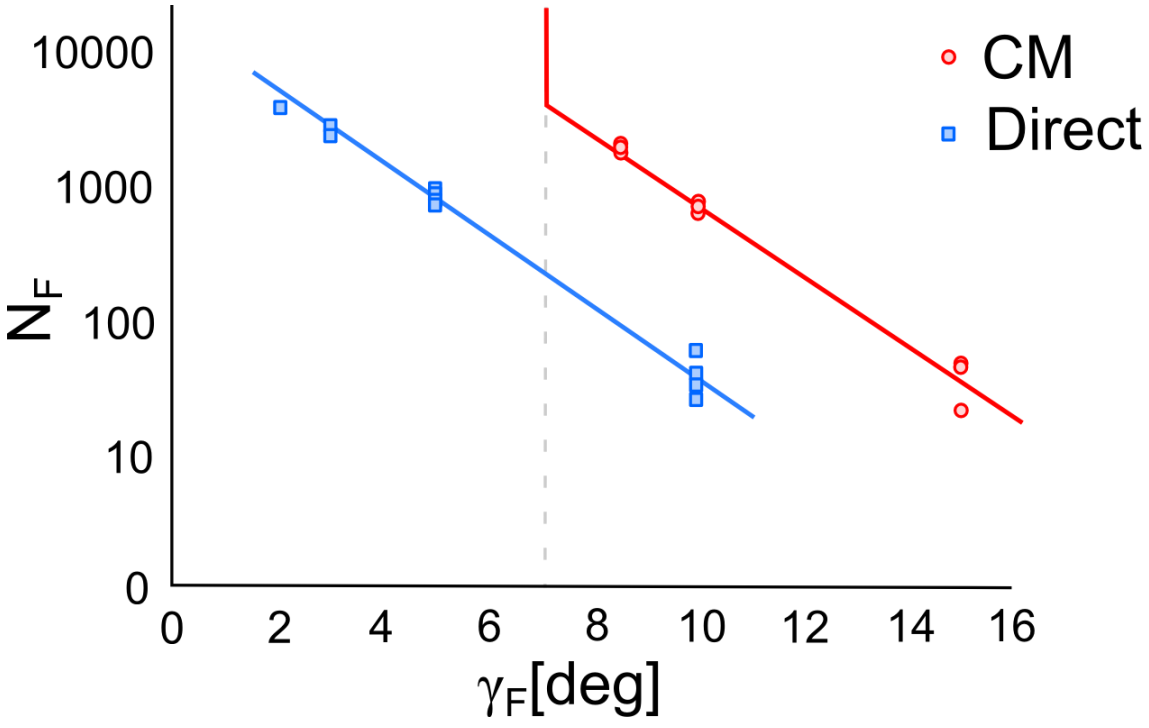

Figure 9